Fast silicon photomultiplier improves signal harvesting and reduces complexity in time-domain diffuse optics

Alberto Dalla Mora,[1] Edoardo Martinenghi,[1] Davide Contini,[1,*] Alberto Tosi,[2] Gianluca Boso,[2] Turgut Durduran,[3] Simon Arridge,[4] Fabrizio Martelli,[5] Andrea Farina,[6] Alessandro Torricelli,[1] and Antonio Pifferi[1,6]

[1]*Politecnico di Milano, Dipartimento di Fisica, Milano, Italy*
[2]*Politecnico di Milano, Dipartimento di Elettronica, Informazione e Bioingegneria, Milano, Italy*
[3]*ICFO-Institut de Ciències Fotòniques, Castelldefels (Barcelona), Spain*
[4]*University College London, Department of Computer Science, London, UK*
[5]*Università degli Studi di Firenze, Dipartimento di Fisica e Astronomia, Sesto Fiorentino, Firenze, Italy*
[6]*Consiglio Nazionale delle Ricerche, Istituto di Fotonica e Nanotecnologie, Milano, Italy*
**davide.contini@polimi.it*

Abstract: We present a proof of concept prototype of a time-domain diffuse optics probe exploiting a fast Silicon PhotoMultiplier (SiPM), featuring a timing resolution better than 80 ps, a fast tail with just 90 ps decay time-constant and a wide active area of 1 mm^2. The detector is hosted into the probe and used in direct contact with the sample under investigation, thus providing high harvesting efficiency by exploiting the whole SiPM numerical aperture and also reducing complexity by avoiding the use of cumbersome fiber bundles. Our tests also demonstrate high accuracy and linearity in retrieving the optical properties and suitable contrast and depth sensitivity for detecting localized inhomogeneities. In addition to a strong improvement in both instrumentation cost and size with respect to legacy solutions, the setup performances are comparable to those of state-of-the-art time-domain instrumentation, thus opening a new way to compact, low-cost and high-performance time-resolved devices for diffuse optical imaging and spectroscopy.

OCIS codes: (030.5260) Photon counting; (040.6070) Solid state detectors; (120.4640) Optical instruments; (170.5280) Photon migration; (290.7050) Turbid media; (300.6500) Spectroscopy, time-resolved.

References and links

1. B. Dolgoshein, V. Balagura, P. Buzhan, M. Danilov, L. Filatov, E. Garutti, M. Groll, A. Ilyin, V. Kantserov, V. Kaplin, A. Karakash, F. Kayumov, S. Klemin, V. Korbel, H. Meyer, R. Mizuk, V. Morgunov, E. Novikov, P. Pakhlov, E. Popova, V. Rusinov, F. Sefkow, E. Tarkovsky, and I. Tikhomirov, "Status report on silicon photomultiplier development and its applications," Nucl. Instruments Methods Phys. Res. Sect. A Accel. Spectrometers, Detect. Assoc. Equip. **563**(2), 368–376 (2006).
2. D. Renker, "New trends on photodetectors," Nucl. Instrum. Methods Phys. Res. A **571**(1-2), 1–6 (2007).
3. P. Buzhan, B. Dolgoshein, L. Filatov, A. Ilyin, V. Kantzerov, V. Kaplin, A. Karakash, F. Kayumov, S. Klemin, E. Popova, and S. Smirnov, "Silicon photomultiplier and its possible applications," Nucl. Instrum. Methods Phys. Res. A **504**(1-3), 48–52 (2003).
4. C. Zhang, L. Zhang, R. Yang, K. Liang, and D. Han, "Time-correlated Raman and fluorescence spectroscopy based on a silicon photomultiplier and time-correlated single photon counting technique," Appl. Spectrosc. **67**(2), 136–140 (2013).
5. T. Durduran, R. Choe, W. B. Baker, and A. G. Yodh, "Diffuse optics for tissue monitoring and tomography," Rep. Prog. Phys. **73**(7), 076701 (2010).
6. A. Torricelli, D. Contini, A. Pifferi, M. Caffini, R. Re, L. Zucchelli, and L. Spinelli, "Time domain functional NIRS imaging for human brain mapping," Neuroimage **85**(Pt 1), 28–50 (2014).
7. F. Scholkmann, S. Kleiser, A. J. Metz, R. Zimmermann, J. Mata Pavia, U. Wolf, and M. Wolf, "A review on continuous wave functional near-infrared spectroscopy and imaging instrumentation and methodology," Neuroimage **85**(Pt 1), 6–27 (2014).

#235680 - $15.00 USD Received 6 Mar 2015; revised 24 Apr 2015; accepted 30 Apr 2015; published 19 May 2015

8. A. T. Eggebrecht, S. L. Ferradal, A. Robichaux-Viehoever, M. S. Hassanpour, H. Dehghani, A. Z. Snyder, T. Hershey, and J. P. Culver, "Mapping distributed brain function and networks with diffuse optical tomography," Nat. Photonics **8**(6), 448–454 (2014).
9. M. Wolf, M. Ferrari, and V. Quaresima, "Progress of near-infrared spectroscopy and topography for brain and muscle clinical applications," J. Biomed. Opt. **12**(6), 062104 (2007).
10. A. Pifferi, A. Farina, A. Torricelli, G. Quarto, R. Cubeddu, and P. Taroni, "Review: Time-domain broadband near infrared spectroscopy of the female breast: a focused review from basic principles to future perspectives," J. Near Infrared Spectrosc. **20**(1), 223–235 (2012).
11. R. Choe, A. Corlu, K. Lee, T. Durduran, S. D. Konecky, M. Grosicka-Koptyra, S. R. Arridge, B. J. Czerniecki, D. L. Fraker, A. DeMichele, B. Chance, M. A. Rosen, and A. G. Yodh, "Diffuse optical tomography of breast cancer during neoadjuvant chemotherapy: A case study with comparison to MRI," Med. Phys. **32**(4), 1128–1139 (2005).
12. A. Torricelli, L. Spinelli, D. Contini, M. Vanoli, A. Rizzolo, and P. Eccher Zerbini, "Time-resolved reflectance spectroscopy for non-destructive assessment of food quality," Sens. Instrumen. Food Qual. **2**(2), 82–89 (2008).
13. I. Bargigia, A. Nevin, A. Farina, A. Pifferi, C. D'Andrea, M. Karlsson, P. Lundin, G. Somesfalean, and S. Svanberg, "Diffuse optical techniques applied to wood characterisation," J. Near Infrared Spectrosc. **21**(4), 259–268 (2013).
14. D. Khoptyar, A. A. Subash, S. Johansson, M. Saleem, A. Sparén, J. Johansson, and S. Andersson-Engels, "Broadband photon time-of-flight spectroscopy of pharmaceuticals and highly scattering plastics in the VIS and close NIR spectral ranges," Opt. Express **21**(18), 20941–20953 (2013).
15. T. Svensson, K. Vynck, E. Adolfsson, A. Farina, A. Pifferi, and D. S. Wiersma, "Light diffusion in quenched disorder: role of step correlations," Phys. Rev. E Stat. Nonlin. Soft Matter Phys. **89**(2), 022141 (2014).
16. S. Mandai and E. Charbon, "Multi-channel digital SiPMs: concept, analysis and implementation," Proc. of IEEE Nuclear Science Symposium and Medical Imaging Conference, 1840–1844 (2012).
17. F. Villa, D. Bronzi, M. Vergani, Y. Zou, A. Ruggeri, F. Zappa, and A. Dalla Mora, "Analog SiPM in planar CMOS technology," Proceedings of ESSDERC, 294–297 (2014).
18. R. Zimmermann, F. Braun, T. Achtnich, O. Lambercy, R. Gassert, and M. Wolf, "Silicon photomultipliers for improved detection of low light levels in miniature near-infrared spectroscopy instruments," Biomed. Opt. Express **4**(5), 659–666 (2013).
19. D. Sanfilippo, G. Valvo, M. Mazzillo, A. Piana, B. Carbone, L. Renna, P. G. Fallica, D. Agrò, G. Morsellino, M. Pinto, R. Canicattì, N. Galioto, A. Tomasino, G. Adamo, S. Stivala, A. Parisi, L. Curcio, C. Giaconia, A. C. Busacca, R. Pagano, S. Libertino, and S. Lombardo, "Design and development of a fNIRS system prototype based on SiPM detectors," Proc. SPIE **8990**, 899016 (2014).
20. H. Wabnitz, D. R. Taubert, M. Mazurenka, O. Steinkellner, A. Jelzow, R. Macdonald, D. Milej, P. Sawosz, M. Kacprzak, A. Liebert, R. Cooper, J. Hebden, A. Pifferi, A. Farina, I. Bargigia, D. Contini, M. Caffini, L. Zucchelli, L. Spinelli, R. Cubeddu, and A. Torricelli, "Performance assessment of time-domain optical brain imagers, part 1: basic instrumental performance protocol," J. Biomed. Opt. **19**(8), 086010 (2014).
21. A. Pifferi, A. Torricelli, A. Bassi, P. Taroni, R. Cubeddu, H. Wabnitz, D. Grosenick, M. Möller, R. Macdonald, J. Swartling, T. Svensson, S. Andersson-Engels, R. L. P. van Veen, H. J. C. M. Sterenborg, J.-M. Tualle, H. L. Nghiem, S. Avrillier, M. Whelan, and H. Stamm, "Performance assessment of photon migration instruments: the MEDPHOT protocol," Appl. Opt. **44**(11), 2104–2114 (2005).
22. H. Wabnitz, A. Jelzow, M. Mazurenka, O. Steinkellner, R. Macdonald, D. Milej, N. Żołek, M. Kacprzak, P. Sawosz, R. Maniewski, A. Liebert, S. Magazov, J. Hebden, F. Martelli, P. Di Ninni, G. Zaccanti, A. Torricelli, D. Contini, R. Re, L. Zucchelli, L. Spinelli, R. Cubeddu, and A. Pifferi, "Performance assessment of time-domain optical brain imagers, part 2: nEUROPt protocol," J. Biomed. Opt. **19**(8), 086012 (2014).
23. A. Tosi, A. Dalla Mora, A. Della Frera, F. Acerbi, A. Bahgat Shehata, and F. Zappa, "Advanced single photon counting instrumentation for SPADs," Proc. SPIE **7945**, 79452 (2011).
24. K. Johnson, M. Hibbs-Brenner, W. Hogan, and M. Dummer, "Advances in red VCSEL technology," Adv. Opt. Technol. **2012**, 1–13 (2012).
25. A. Dalla Mora, D. Contini, S. Arridge, F. Martelli, A. Tosi, G. Boso, A. Farina, T. Durduran, E. Martinenghi, A. Torricelli, and A. Pifferi, "Towards next-generation time-domain diffuse optics for extreme depth penetration and sensitivity," Biomed. Opt. Express **6**(5), 1749–1760 (2015).
26. F. Acerbi, A. Ferri, A. Gola, M. Cazzanelli, L. Pavesi, N. Zorzi, and C. Piemonte, "Characterization of single-photon time resolution: from single SPAD to silicon photomultiplier," IEEE Trans. Nucl. Sci. **61**(5), 2678–2686 (2014).
27. D. Contini, A. Dalla Mora, L. Spinelli, A. Farina, A. Torricelli, R. Cubeddu, F. Martelli, G. Zaccanti, A. Tosi, G. Boso, F. Zappa, and A. Pifferi, "Effects of time-gated detection in diffuse optical imaging at short source-detector separation," J. Phys. D Appl. Phys. **48**(4), 045401 (2015).
28. R. Re, D. Contini, M. Turola, L. Spinelli, L. Zucchelli, M. Caffini, R. Cubeddu, and A. Torricelli, "Multi-channel medical device for time domain functional near infrared spectroscopy based on wavelength space multiplexing," Biomed. Opt. Express **4**(10), 2231–2246 (2013).
29. D. Contini, F. Martelli, and G. Zaccanti, "Photon migration through a turbid slab described by a model based on diffusion approximation. I. Theory," Appl. Opt. **36**(19), 4587–4599 (1997).
30. W. H. Press, S. A. Teukolsky, W. T. Vetterling, and B. P. Flannery, Numerical Recipes in C: the Art of Scientific Computing (Cambridge University Press, Cambridge, UK, 1992).
31. F. Martelli, A. Pifferi, D. Contini, L. Spinelli, A. Torricelli, H. Wabnitz, R. Macdonald, A. Sassaroli, and G. Zaccanti, "Phantoms for diffuse optical imaging based on totally absorbing objects, part 1: Basic concepts," J. Biomed. Opt. **18**(6), 066014 (2013).

#235680 - $15.00 USD Received 6 Mar 2015; revised 24 Apr 2015; accepted 30 Apr 2015; published 19 May 2015

32. F. Martelli and G. Zaccanti, "Calibration of scattering and absorption properties of a liquid diffusive medium at NIR wavelengths. CW method," Opt. Express **15**(2), 486–500 (2007).
33. R. Michels, F. Foschum, and A. Kienle, "Optical properties of fat emulsions," Opt. Express **16**(8), 5907–5925 (2008).
34. L. Spinelli, F. Martelli, A. Farina, A. Pifferi, A. Torricelli, R. Cubeddu, and G. Zaccanti, "Calibration of scattering and absorption properties of a liquid diffusive medium at NIR wavelengths. Time-resolved method," Opt. Express **15**(11), 6589–6604 (2007).
35. L. Spinelli, M. Botwicz, N. Zolek, M. Kacprzak, D. Milej, P. Sawosz, A. Liebert, U. Weigel, T. Durduran, F. Foschum, A. Kienle, F. Baribeau, S. Leclair, J.-P. Bouchard, I. Noiseux, P. Gallant, O. Mermut, A. Farina, A. Pifferi, A. Torricelli, R. Cubeddu, H.-C. Ho, M. Mazurenka, H. Wabnitz, K. Klauenberg, O. Bodnar, C. Elster, M. Bénazech-Lavoué, Y. Bérubé-Lauzière, F. Lesage, D. Khoptyar, A. A. Subash, S. Andersson-Engels, P. Di Ninni, F. Martelli, and G. Zaccanti, "Determination of reference values for optical properties of liquid phantoms based on Intralipid and India ink," Biomed. Opt. Express **5**(7), 2037–2053 (2014).
36. A. I. R. Maas and G. Citerio, "Noninvasive monitoring of cerebral oxygenation in traumatic brain injury: a mix of doubts and hope," Intensive Care Med. **36**(8), 1283–1285 (2010).
37. A. Ghosh, C. Elwell, and M. Smith, "Review article: cerebral near-infrared spectroscopy in adults: a work in progress," Anesth. Analg. **115**(6), 1373–1383 (2012).
38. M. S. Patterson, B. Chance, and B. C. Wilson, "Time resolved reflectance and transmittance for the non-invasive measurement of tissue optical properties," Appl. Opt. **28**(12), 2331–2336 (1989).
39. J. Steinbrink, H. Wabnitz, H. Obrig, A. Villringer, and H. Rinneberg, "Determining changes in NIR absorption using a layered model of the human head," Phys. Med. Biol. **46**(3), 879–896 (2001).
40. J. Selb, J. J. Stott, M. A. Franceschini, A. G. Sorensen, and D. A. Boas, "Improved sensitivity to cerebral hemodynamics during brain activation with a time-gated optical system: analytical model and experimental validation," J. Biomed. Opt. **10**(1), 011013 (2005).
41. A. Torricelli, A. Pifferi, L. Spinelli, R. Cubeddu, F. Martelli, S. Del Bianco, and G. Zaccanti, "Time-resolved reflectance at null source-detector separation: improving contrast and resolution in diffuse optical imaging," Phys. Rev. Lett. **95**(7), 078101 (2005).
42. A. Pifferi, A. Torricelli, L. Spinelli, D. Contini, R. Cubeddu, F. Martelli, G. Zaccanti, A. Tosi, A. Dalla Mora, F. Zappa, and S. Cova, "Time-resolved diffuse reflectance using small source-detector separation and fast single-photon gating," Phys. Rev. Lett. **100**(13), 138101 (2008).
43. E. Alerstam, T. Svensson, S. Andersson-Engels, L. Spinelli, D. Contini, A. Dalla Mora, A. Tosi, F. Zappa, and A. Pifferi, "Single-fiber diffuse optical time-of-flight spectroscopy," Opt. Lett. **37**(14), 2877–2879 (2012).
44. A. Tosi, A. Dalla Mora, F. Zappa, A. Gulinatti, D. Contini, A. Pifferi, L. Spinelli, A. Torricelli, and R. Cubeddu, "Fast-gated single-photon counting technique widens dynamic range and speeds up acquisition time in time-resolved measurements," Opt. Express **19**(11), 10735–10746 (2011).
45. G. Boso, A. Dalla Mora, A. Della Frera, and A. Tosi, "Fast-gating of single-photon avalanche diodes with 200 ps transitions and 30 ps timing jitter," Sens. Actuators A Phys. **191**, 61–67 (2013).
46. M. Buttafava, G. Boso, A. Ruggeri, A. Dalla Mora, and A. Tosi, "Time-gated single-photon detection module with 110 ps transition time and up to 80 MHz repetition rate," Rev. Sci. Instrum. **85**(8), 083114 (2014).
47. F. Villa, B. Markovic, S. Bellisai, D. Bronzi, A. Tosi, F. Zappa, S. Tisa, D. Durini, S. Weyers, U. Paschen, and W. Brockherde, "SPAD smart pixel for time-of-flight and time-correlated single-photon counting measurements," IEEE Photonics J. **4**(3), 795–804 (2012).
48. T. Frach, G. Prescher, C. Degenhardt, R. de Gruyter, A. Schmitz, and R. Ballizany, "The digital silicon photomultiplier - Principle of operation and intrinsic detector performance," 2009 IEEE Nuclear Science Symposium Conference Record, 1959–1965 (2009).
49. A. Dalla Mora, A. Tosi, F. Zappa, S. Cova, D. Contini, A. Pifferi, L. Spinelli, A. Torricelli, and R. Cubeddu, "Fast-gated single-photon avalanche diode for wide dynamic range near infrared spectroscopy," IEEE J. Sel. Top. Quantum Electron. **16**(4), 1023–1030 (2010).
50. A. Dalla Mora, A. Tosi, S. Tisa, and F. Zappa, "Single-photon avalanche diode model for circuit simulations," IEEE Photon. Technol. Lett. **19**(23), 1922–1924 (2007).

1. Introduction

A Silicon PhotoMultiplier (SiPM) consists of an array of hundreds (or thousands) microcells, each one including a Single-Photon Avalanche Diode (SPAD) and its passive quenching resistor. All microcells are connected in parallel with very high fill-factor (typically > 60%), thus forming a single global anode and a single global cathode [1,2]. The device outputs an analog pulse with amplitude proportional to the number of microcells in which the avalanche has been triggered by a single photon. This feature makes the device useful for both single-photon counting and multi-photon applications. The impressive development of SiPM technology in the last decade has been mainly led by high-energy physics (e.g. positron emission tomography scanners, Cherenkov telescopes, etc.) [3], where they are coupled to scintillators, aiming at replacing bulky, fragile and expensive photocathode-based detectors like PhotoMultiplier Tubes (PMTs). The requirement of large detector panels, composed of thousands of SiPMs, led to continuous improvement in performance and reduction in cost.

#235680 - $15.00 USD Received 6 Mar 2015; revised 24 Apr 2015; accepted 30 Apr 2015; published 19 May 2015

SiPMs are rapidly expanding their fields of use encompassing also other applications requiring detection of low light levels (close to the single-photon level) with great efficiency, such as fluorescence and Raman spectroscopy [4].

Another potential application for SiPM is within the field of diffuse optics. The study of photon migration in highly scattering media – e.g. biological tissues – conveys information on the absorption and scattering properties of the medium explored by photons along their paths. Diffuse optics [5] is a powerful tool in many applications like functional brain imaging [6–8], oximetry [9], mammography [10], monitoring of neoadjuvant chemotherapy [11], quality assessment of food [12], wood [13], pharmaceuticals [14], investigations of photon migration in random media [15] and many others.

SiPMs are particularly attractive for replacing PMTs or hybrid PMTs in diffuse optics due to their: (*i*) wide active area (up to few mm^2) and (*ii*) numerical aperture (in principle close to 1), both directly reflecting into high photon collection efficiency; (*iii*) high quantum efficiency (e.g. > 20% at 600 nm wavelength); (*iv*) broad spectral coverage (350 - 1000 nm); (*v*) low cost (~100 $ for single off-the-shelf devices); (*vi*) compactness (because of the very basic electronics needed to operate them thanks to the integrated resistor); (*vii*) robustness (they are not sensitive to electromagnetic fields or strong light exposure); (*viii*) versatility (they do not require cooling systems); (*ix*) Complementary Metal-Oxide Semiconductor (CMOS) technology compatibility [16,17].

Because of the previous advantages, during the last two years the diffuse optics community started to consider SiPMs to build Continuous-Wave (CW) prototypes for functional Near-Infrared Spectroscopy (fNIRS) [18,19]. On the other side, despite the great attractiveness of SiPMs, their use in Time Domain (TD) diffuse optics is still largely unexplored. It has long been assumed that SiPMs were unsuitable for TD diffuse optics because of the high background noise, overwhelming the weak optical signal and saturating the Time-Correlated Single-Photon Counting (TCSPC) electronics. Also, strong afterpulsing was cause of additional signal-related increase in background noise. Furthermore, until recently, the temporal resolution of commercially available devices seemed not adequate for TD diffuse optics (being typically > 200 ps). Finally, most SiPM devices are optimized for use in multi-photon regime, thus being unsuitable in TCSPC schemes. For all these reasons, the impressive development of SiPM technology was somewhat neglected by the diffuse optics scientific community.

In this paper we demonstrate for the first time that targeted selection of commercially-available SiPM devices combined with proper dedicated electronics permits to overcome the key limitations of SiPMs for TD diffuse optics, prefiguring a new powerful general-purpose TD detector with fascinating perspectives towards compact, low cost, and wearable devices, on one side and powerful, multi-optode, tomographic probes on the other side.

In the following, we will first describe the experimental setup employed to implement the SiPM-based TD device. Then, the aptness and versatility of the detector for TD diffuse optics at large is demonstrated using a set of internationally adopted protocols for performance assessment. The device is tested against basic instrument performance to check the suitability of the detector response and the improvement in light harvesting (BIP Protocol) [20]. Then the capability to retrieve the absorption and scattering properties in homogenous media for spectroscopy measurements is assessed (MEDPHOT Protocol) [21]. Finally, the performance in detecting a localised absorption inhomogeneity in depth within a semi-infinite diffusive medium is measured for imaging purposes (nEUROPt Protocol) [22].

2. Optical probe and setup

A photograph of the developed detection optode for TD diffuse optics is shown in Fig. 1. The printed circuit board hosts a SiPM as free-running time-resolved detector (Part number C30742-11-050-C, Excelitas Technologies, Canada) together with its basic front-end circuit. The detector active area is composed by 400 square microcells having 50 μm sides each, thus reaching a 1 mm^2 squared active area. Its photon detection efficiency is higher than 10% around 690 nm wavelength. The simple front-end circuit shown in Fig. 1 is composed by: *i*) a

#235680 - $15.00 USD Received 6 Mar 2015; revised 24 Apr 2015; accepted 30 Apr 2015; published 19 May 2015

resistor for avalanche current sensing; *ii*) a capacitor for picking-up the avalanche pulse without affecting the detector steady-state bias; *iii*) some additional capacitors for stabilizing the detector bias voltage. Both board layout and components must follow high-frequency design rules to avoid detrimental effects on the very faint single-photon avalanche signal. While the front-end circuit plays an important role for the single-photon timing performance, it has an almost negligible effect on the device performances in terms of both dark count rate and afterpulsing reduction since the SiPM integrated quenching resistors are dominant. The reported improvement in background noise is only due to the targeted selection of commercially-available SiPM devices.

Figure 2 shows the whole instrumental setup employed for the following experiments. A fast pulse generator (custom design of Politecnico di Milano [23]) provides 220 ps gating pulses with 7 V amplitude at the repetition rate of 40 MHz to a Vertical-Cavity Surface-Emitting Laser (VCSEL) source [24], thus triggering a fast stimulated emission of carriers from the laser energy level (gain-switching operation). The pulsed VCSEL (Part number 680C, Vixar Inc., USA) provides 250 ps full-width at half maximum (FWHM) pulses at 690 nm with up to 900 μW average power. The design and characterization of the laser source is detailed in [25]. The pulse generator also provides a global synchronization signal for the whole system. A low-noise signal amplifier (VT120, Ortec, USA) is employed to increase the amplitude of the SiPM avalanche transient for the following stage in order to be able to reach the ultimate timing performance from the device. A Time-Correlated Single-Photon Counting (TCSPC) board (SPC-130, Becker & Hickl GmbH, Germany), hosted into a personal computer, builds the histogram of the single-photons arrival times. Finally, few commercial power supplies are used to bias the entire system.

3. Basic instrument performance assessment (BIP protocol)

In order to demonstrate the suitability of timing performance of the SiPM-based detection system, we acquired its response function to a fast laser pulse (with almost negligible time duration with respect to the SiPM response) generated by a photonic crystal fiber laser (SC450, Fianium Ltd, UK) emitting supercontinuum light at the repetition rate of 40 MHz and with few picoseconds pulse duration. Wavelength dispersion and selection are achieved by means of a computer-controlled rotation of a prism.

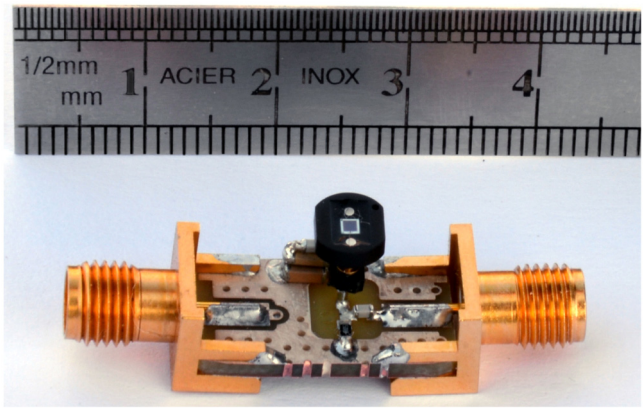

Fig. 1. Photograph of the developed compact optode based on a silicon photomultiplier.

#235680 - $15.00 USD Received 6 Mar 2015; revised 24 Apr 2015; accepted 30 Apr 2015; published 19 May 2015

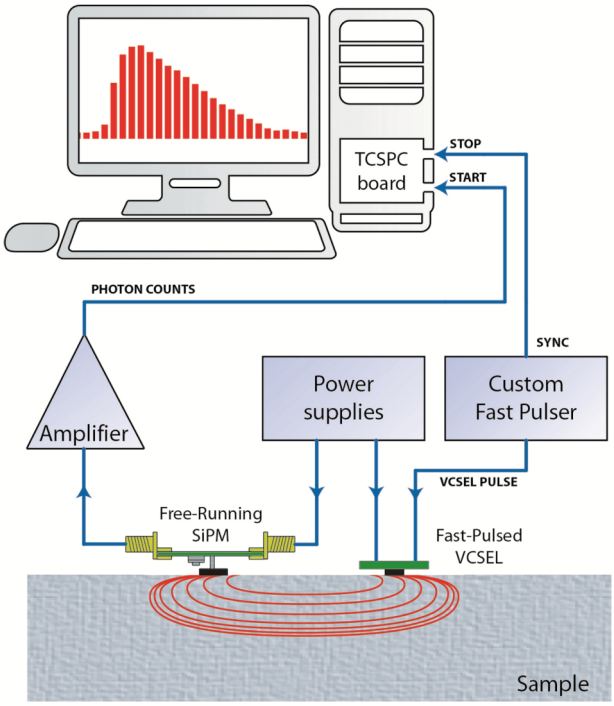

Fig. 2. Scheme of the experimental setup employed: a pulse generator provides voltage pulses to a VCSEL and a synchronization signal for the system; a signal amplifier increases the amplitude of the SiPM avalanche transient; a PC-hosted TCSPC board builds the histogram of the photon time-of-flights.

Figure 3 (solid line) shows the single-photon timing response at 690 nm, featuring a remarkable timing resolution of 77 ps FWHM, which is at the level of the record results recently reported in literature for similar devices [26]. A first tail in the temporal response is very fast, featuring about 90 ps time-constant, thus enabling to accurately measure optical temporal decays [27]. A secondary long tail with nanoseconds time constant starts about 3 decades below the peak, thus limiting the dynamic range to 3 orders of magnitude. We verified that both timing resolution and tail time constants are almost independent of the wavelength in a wide spectral range, ranging from 600 to above 1000 nm, thus enabling the use of this kind of detector for broadband TD diffuse spectroscopy.

Following the BIP protocol for basic instrument performance assessment [20], we characterized the Instrument Response Function (IRF) of the system shown in Fig. 2, which includes the pulsed VCSEL as light source. The IRF is shown in Fig. 3 (dotted line) and it has been achieved by directly facing source and detector, with a thin Teflon layer in-between so to ensure the uniform and isotropic illumination of the latter. The achieved timing resolution of the system is about 280 ps FWHM, mainly related to the VCSEL pulse width and comparable with many other state of the art TD diffuse optical systems [6]. The bump observed at 1.6 ns is due to a VCSEL relaxation oscillation.

An important parameter that can be measured to characterize the overall efficiency of a diffuse optical instrumentation to both collect and detect back-diffused light from a sample is the so-called responsivity, specifically defined in BIP for light harvesting from a diffusive medium [20]. Generally speaking, with respect to a simple photon detection efficiency measurement, the responsivity test takes also into account the effective detector numerical aperture, and all losses in the optical chain. We measured it by following the procedure described in [20], which is based on a calibrated solid phantom. With the purpose to avoid the use of optical fibers, the SiPM is directly placed in contact with the phantom. At 690 nm

#235680 - $15.00 USD Received 6 Mar 2015; revised 24 Apr 2015; accepted 30 Apr 2015; published 19 May 2015

wavelength, the measured responsivity value is 5.83•107 m2sr. This result is remarkable since it demonstrates a gain of more than one order of magnitude with respect to state-of-the-art devices based on cumbersome 3 mm core fiber bundles and Hybrid PMTs [28], where just 4.29•10□8 m2sr has been measured at 687 nm following the same procedure. The motivation of this improvement can be mainly found in the larger numerical aperture (NA) of the SiPM (NA ~1) with respect to the fiber bundle used in the reference system (NA = 0.57), as well as in the reduction of photon losses by avoiding optical components, like lenses, along the detection channel.

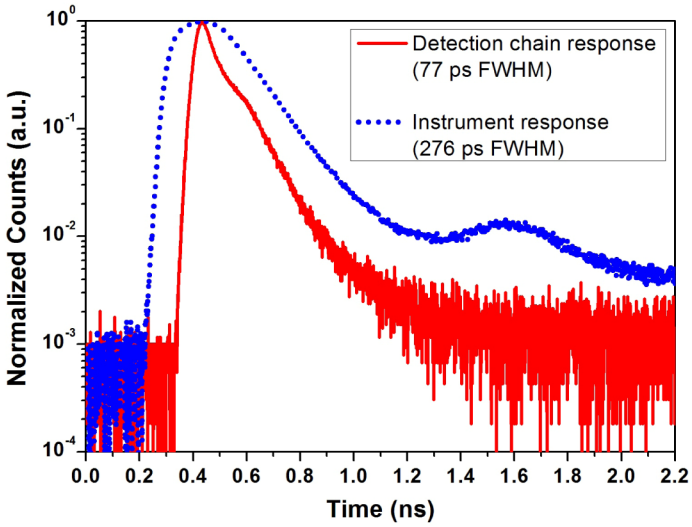

Fig. 3. Single-photon timing response at 690 nm of the SiPM-based detection system when stimulated by a picosecond laser pulse (solid line). Global instrument response function using pulsed VCSEL at 690 nm (dotted line).

4. Measurement of optical properties (MEDPHOT protocol)

We tested the instrument performance in retrieving the optical properties of homogeneous solid phantoms based on TiO_2 powder as diffusive medium and on toner powder as absorber, both inserted into an epoxy resin mould. Following the MEDPHOT protocol [21], a series of 32 solid phantoms covering optical properties in the range 0 - 0.5 cm^{-1} for the absorption coefficient (μ_a) and 5 - 20 cm^{-1} for the reduced scattering coefficient (μ_s') is measured at 690 nm wavelength with an acquisition time of 20 s each, using a 3 cm source-detector separation. This experiment is expected to give information on the achievable linearity and accuracy in the assessment of the optical properties.

The optical properties are retrieved by fitting the time-resolved reflectance waveform with the analytical solution of the diffusion approximation of the transport equation (previously convoluted with the IRF), by using extrapolated boundary conditions for an infinite homogeneous slab (see [29], Contini *et al.* for further details). The fitting range is set in order to exclude the portion of the curve rising edge showing a number of counts lower than 10% of the peak value, while the limit on the falling edge is 1%. A standard Levenberg-Marquardt algorithm is selected for the fitting process [30].

Results on the 32 phantoms are reported in Fig. 4. Data show a very good linearity and accuracy over the whole wide absorption and scattering range, thus proving the SiPM aptness for many applications (e.g. breast density assessment, fruit maturity staging, etc.) where just spectroscopic average properties are needed.

#235680 - $15.00 USD Received 6 Mar 2015; revised 24 Apr 2015; accepted 30 Apr 2015; published 19 May 2015

5. Contrast measurements (nEUROPt protocol)

To validate the developed system also for inhomogeneous problems, following the nEUROPt protocol [22], we measured the contrast produced by a black cylinder with 100 mm^3 volume (5 mm diameter and 5 mm height). As demonstrated in [31] by Martelli *et al.*, the inclusion can properly mimic an equivalent 160% absorption increase over a 1 cm^3 volume. The center of the cylinder is placed at a depth z within a homogeneous liquid phantom based on a water dilution of Intralipid-20% as diffusive medium and India ink as absorber. The reduced scattering coefficient for Intralipid and the absorption coefficient for ink have been widely characterized, using both CW apparatuses [32,33] and TD systems [34], reaching a consensus estimate among many laboratories worldwide better than 3% [35]. For the following measurements, a liquid phantom with μ_a = 0.1 cm^{-1} and μ_s' = 10 cm^{-1} is employed as bulk medium in which the perturbation is placed.

Both VCSEL and SiPM boards were waterproofed by inserting them into a transparent cellophane small bag. They were placed in contact with the free surface of the liquid phantom at a relative distance ρ of 3 cm. The black cylinder is moved at different z depths (ranging from 2.5 mm to 40 mm) into the medium, right in the middle between source and detector. For each position, a reflectance curve is acquired for 10 s.

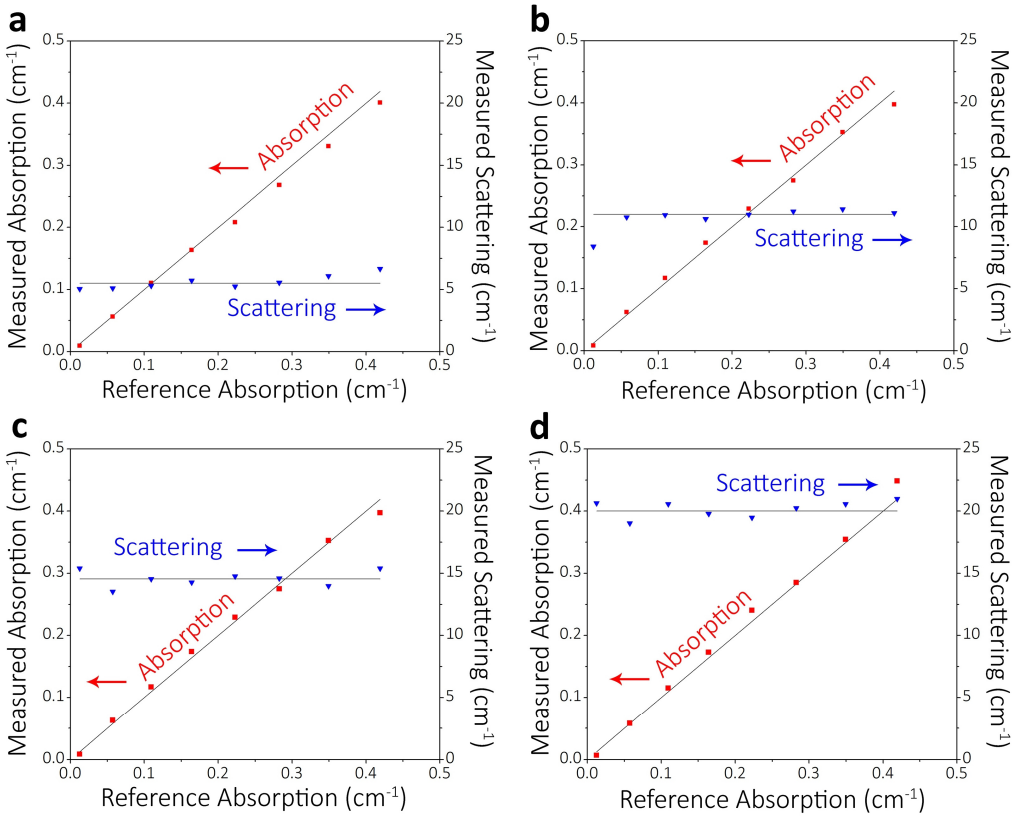

Fig. 4. Measured absorption coefficient (squares) and reduced scattering coefficient (triangles) as a function of the reference absorption coefficient for phantoms with nominal reduced scattering coefficient of 5.5 cm^{-1} (a); 10 cm^{-1} (b), 14.5 cm^{-1} (c), 20 cm^{-1} (d). Reference values have been obtained using time-resolved broadband diffuse optics spectrometers with top-class performances [21]. In each panel, the oblique and horizontal lines represent the reference values for the absorption and reduced scattering coefficients, respectively.

#235680 - $15.00 USD Received 6 Mar 2015; revised 24 Apr 2015; accepted 30 Apr 2015; published 19 May 2015

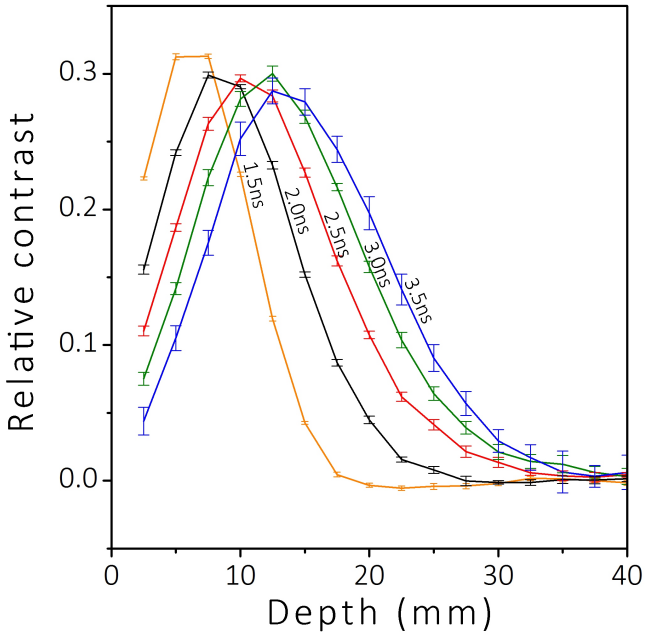

Fig. 5. Average and standard deviation over 10 repetitions of the relative contrast produced by the cylinder as a function of depth from the surface, calculated within a time window of 500 ps starting at different delays with respect to the peak of the IRF.

The relative contrast C produced with respect to the unperturbed situation (i.e. inclusion at 50 mm depth) is calculated within a time window of 500 ps starting at different delays with respect to the peak of the IRF (from 1.5 ns to 3.5 ns at 0.5 ns step). It was evaluated as $C = (N_0\text{-}N)/N_0$, where N_0 is the total number of counts within the selected temporal window for the unperturbed case, while N is the same entity for the perturbed case.

Results are reported in Fig. 5. As expected, as the delay between the peak of the IRF and the opening of the temporal window for contrast calculation increases, the sensitivity of the system is moved towards deeper regions due to the selection of later arriving photons. The probe can detect with $C > 1\%$ down to a remarkable depth of 3 cm. Hence, it can be concluded that the system can sense at a depth of adult brain cortex (i.e. $z > 2$ cm). These figures are comparable with those obtained using state-of-the-art bulky diffuse optics instruments, as reported for instance in the recent inter-laboratory comparison of brain imagers [22].

6. Discussion

The experimental characterization performed on the time-resolved diffuse optics probe based on SiPM, already in this first implementation, demonstrates the suitability of this kind of detector to potentially replace PMTs or hybrid PMTs in TD diffuse optical imaging and spectroscopy.

A CW diffuse optics equipment is usually compact and cheap, but suffers from poor depth sensitivity and accuracy [36,37]. Vice versa, TD instrumentation is recognized to potentially lead to better performance by providing information about photons travelling time [38,39]. Thanks to this feature, a single measurement is sufficient to directly uncouple absorption from scattering contributions, thus leading – for a homogeneous medium – to the absolute quantification of both absorption and reduced scattering coefficients. Further, in the case of reflectance geometry, with light source and detection points placed on the same side of the medium at a relative distance ρ, the mean penetration depth of detected photons steadily increases upon increasing the photon arrival time [39,40], thus permitting deep tissue imaging even at null-ρ [41–43] with the chance to reach a record level of source-detector couples

#235680 - $15.00 USD Received 6 Mar 2015; revised 24 Apr 2015; accepted 30 Apr 2015; published 19 May 2015

coverage to maximize the detected signal and the spatial resolution, provided that an efficient time-gating mechanism is employed to avoid the blinking burst of undesired early-arriving photons [44–46]. However, the main limitations of TD as compared to CW systems during the last two decades have always been high cost and complexity, thus affecting the maximum number of injection and detection channels, and wider deployment of instruments for clinical use. State-of-the-art TD systems are bulky (typically hosted in rack cabinets), expensive (hundreds of thousands dollars), and strongly limited in both number of source-detector pairs (typically < 8) and light harvesting efficiency, thus preventing the full on-the-field exploitation of previous advantages. On the other hand, CW techniques are possibly close to their maximum development due to the impossibility to employ short source-detector separations to increase the number of source-detector pairs. Potentially, TD techniques, allowing small or even null distance between the injection and collection points could overcome the coverage of CW techniques, thus featuring superior performances in terms of spatial resolution and signal to noise ratio. The key point to open the way to the next-generation TD diffuse optical devices is the possibility to exploit novel technologies to develop compact and low-cost basic TD blocks.

Thanks to its architecture, a SiPM requires a very simple front-end electronics, potentially paving the way towards compact and cheap detection channels, with the chance to build multichannel tomographic devices. Being in principle compatible with a standard CMOS process, a single silicon chip could integrate the detector together with all the required electronics (e.g. avalanche pick-up network, amplification stage, etc.) and also a Time-to-Digital Converter (TDC) [47], similarly to the case of present technology of digital SiPM [48]. In this way, a single chip could replace the entire detection channel with striking technological advance. The direct integration of the detector within the probe is a further important step towards the final goal thanks to the reduced complexity, to the increase of the collected signal and to the removal of possible artefacts coming from fiber movements.

7. Conclusions and perspectives

In this work, we have demonstrated for the first time that a selected fast silicon photomultiplier can be profitably employed in time-domain diffuse optics in order to increase the light harvesting with respect to existing solutions, thanks to its wide active area and the possibility to be placed directly onto the probe, in contact with the sample under investigation, so as to strongly reduce complexity of TD instruments. The detector showed low timing jitter, better than 80 ps. The characterization of the TD system based on SiPM demonstrated much better performance compared to state-of-the-art devices in terms of photon collection efficiency. Additionally, we validated it in retrieving the optical properties of homogeneous solid phantoms and for inhomogeneous problems with a localized black solid inclusion placed into a liquid phantom, thus showing performance in line with best in class devices even in this first implementation.

Further development is needed to exploit the full potential of SiPM technology. For instance, up to now SiPMs lack of time-gating capability because of the presence of the integrated quenching resistor that prevents fast rising edges for rapidly turning ON the detector [49,50]. Time-gating by integrating suitable gating circuitry into the SiPM chip would make it possible to use small source-detector separations, thus enabling a dense coverage with many measurement points in order to increase the signal-to-noise ratio. Still, even in the present implementation, SiPMs can easily replace existing detectors in TD diffuse optics and unleash the advantage of TD approaches both at research level, with versatile and powerful multi-optodes probes, and at clinical/industrial level with the deployment of simple, compact and cost-effective devices.

Acknowledgments

The research leading to these results has received funding from the European Community's Seventh Framework Programme under grant agreements nEUROPt n°201076 and LASERLAB EUROPE n°284464.